Multimode Analysis of Transmission Lines and Substrates for (sub)mm-Wave Calibration

M. Spirito, G. Gentile and A. Akhnoukh

Electronics Research Laboratory/DIMES, Delft University of Technology
Mekelweg 4, 2628CD Delft, The Netherlands

***Abstract* — In this contribution we present a numerical and experimental analysis of the multimode propagation over co-planar transmission lines, in order to define guidelines for substrate selection to achieve accurate wafer-level (sub)mm-wave calibrations.**

Losses and coupling effects resulting from the multiple propagating modes on transmission lines conventionally employed for probe-level calibrations, are analysed by means of 3D electro-magnetic simulations.

A low loss-tangent, low dielectric constant material (i.e., fused silica), providing low radiation losses due to mode coupling, is proposed as substrate to achieve accurate (sub)mm-wave calibrations. The structures required to perform a TRL calibration are integrated on the proposed fused silica substrate and the experimental data of probe-level calibration performed in the 220-325GHz band are presented.

***Index Terms* — Surface waves, multimode propagation, dispersion, on-wafer calibration, (sub)mm-wave.**

I. Introduction

The accuracy of high-frequency vector network analyser (VNA) calibration is directly related, in first approximation, to the knowledge of the electrical behaviour of the structures used during the procedure. At (sub)mm-wave frequencies, thru-reflect-line (TRL) is the most employed calibration technique due to the limited requirements on the standards, which are only related to the knowledge of the characteristic impedance of the line and the length of the thru. Moreover, at such high frequencies the small length of the transmission line (i.e., close to λ/4 in the middle of the calibration band) reduces considerably the travelling of the manipulator stages, making it more suitable for probe-level calibration.

Nevertheless, as frequency increases, the fixed limits imposed by mechanical parameters (i.e., substrate height for mechanical manufacturability and line width for reliable probe landing/skating) do not allow to scale proportionally the line and substrate dimensions in order to guarantee single-mode propagation. For this reason it is crucial to analyse the multimode propagation mechanisms occurring on the transmission line, as was shown in [1].

In this paper the different propagation modes supported by coplanar-waveguides used for calibration are first analysed employing 3D electro-magnetic (EM) simulations. After, the conventional procedures to minimize some of the parasitic modes are described. The substrate properties strongly impacting the generation of surface waves are then discussed. Finally, calibrated measured data of structures integrated on a fused silica substrate and alumina substrate are presented and compared to their 3D EM simulations.

II. Multimode Propagation in CPWs

The different propagating modes supported by a CPW are qualitatively sketched in Fig. 1.

The CPW mode characterized by opposite direction of the fields across the slots, represents the intended propagation mode and is often referred to as *CPW differential mode*. The CPW mode characterized by in-phase direction of the field across the slots represents an unwanted radiating mode and is often referred to as *CPW common mode*.

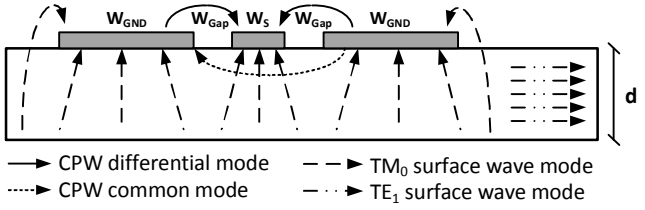

Fig. 1: Cross section of a CPW with finite ground planes, and sketches of the E field distributions of the first propagating modes supported.

The TM_n and TE_n modes are surface waves propagating along the grounded dielectric slab, their cut off frequency is a function of the height and dielectric constant of the substrate, as shown by eq. 1 [2].

$$TM_n: \quad f_c = \frac{n \cdot c}{2 \cdot d \cdot \sqrt{\varepsilon_r - 1}} \qquad n = 0,1,2...$$
$$TE_n: \quad f_c = \frac{(2 \cdot n - 1) \cdot c}{4 \cdot d \cdot \sqrt{\varepsilon_r - 1}} \qquad n = 1,2... \tag{1}$$

The overall effect of the unwanted modes described above is an increase of the transmission line losses (i.e., |S21|) and the generation of ripples on the transmission parameter (i.e., S21) of the CPW. The ripples are the results of interference (constructive or destructive depending on the electrical length) between the unwanted modes, reflected by discontinues (i.e.,

dielectric constant changes), and the intended CPW mode. The various modes propagating in a CPW structure can be identified, by means of numerical 3D EM simulation [3][4], observing the normalized phase constant associated to each mode, as shown in Fig. 2. The figure is generated using a 3D FEM solver, i.e., Ansoft HFSS, employing the values of Table I for the line and substrate parameters. The wanted CPW mode shows low dispersion up to 200GHz, and its low-frequency effective dielectric constant coincides with the one calculated by the well-known equation:

$$\varepsilon_{r,eff} = \frac{\varepsilon_r - 1}{2} \qquad (2)$$

TABLE I: LINE AND SUBSTRATE PARAMETERS – ALUMINA -

Parameter	W_S	W_{Gap}	W_{GND}	d	ε_r
Value (in μm)	47.5	30	125	200	9.9
Metal: perfect electric conductor; *dielectric*: lossless alumina					

As the frequency increases the wanted CPW mode can couple with various (unwanted) dispersive modes.

The cross-over between the dispersive modes and the wanted CPW mode shown in Fig. 2, represent frequency of strong coupling. Reducing the substrate height or dielectric constant allows to shift the cut-off of the TE_1 mode to higher frequencies.

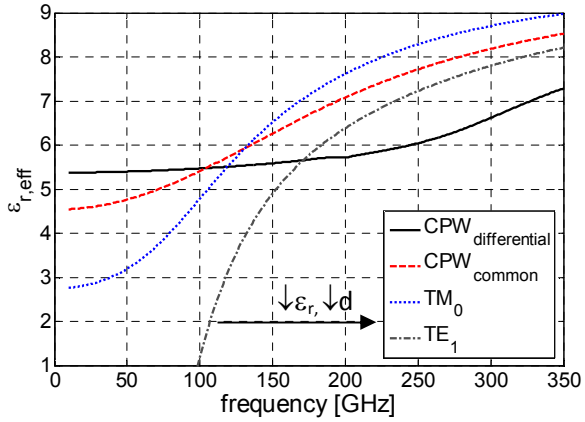

Fig. 2: Dispersion curves of the first propagating modes for the CPW (see Fig. 1) over alumina substrate with finite ground planes.

III. MULTIMODE PROPAGATION IN CALIBRATION CPWS

The lines conventionally employed for on-wafer TRL calibration, are:

- The *thru line*, implemented as a CPW with a physical length in the order of 200-250μm,
- The *line*, implemented as a CPW providing an insertion phase of ~90° at the center of the calibration band.

The analysis presented in this section is based on numerical 3D simulations, employing Agilent EM Pro FEM simulator, and are based on the structure and substrate parameters reported in Table I.

A. Parallel plate waveguide mode

During the calibration procedure the substrate is placed over a metallic wafer chuck, creating effectively a grounded coplanar waveguide (GCPW) structure [1], as shown in Fig. 3 a. This structure supports, in addition to the modes shown in Fig. 1, also a parallel plate waveguide (PPL) mode. This occurs since the top and bottom metal are not directly contacted, thus a different potential can exist and propagate. The PPL mode can be visualized by plotting the E field intensity below the metal surface.

Conventionally to reduce the PPL mode propagation an interposer substrate, of ferromagnetic material (i.e., providing high losses for the EM waves), is used between the calibration substrate and the metal chuck.

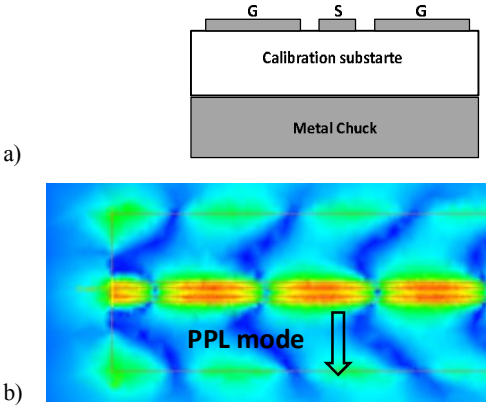

a)

b)

Fig. 3: a) Cross section of CPW on calibration substrate placed on metal chuck, b) top view of the electrical field below the grounded CPW metal plates, computed at 110GHz.

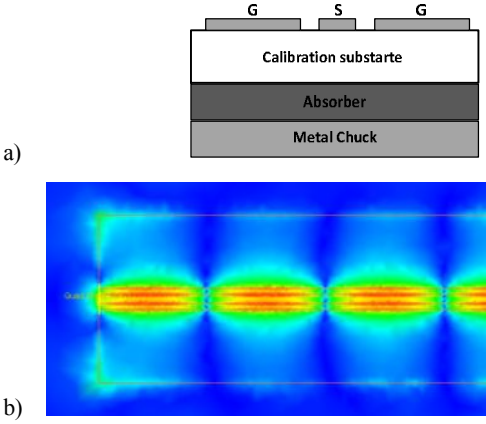

a)

b)

Fig. 4: a) Cross section of CPW on calibration substrate placed on the absorber interposer over the metal chuck, b) top view of the electrical field below the CPW, when using absorbing boundary below the substrate in the 3D FEM simulation, fields computed at 110GHz.

To highlight the decrease in the PPL mode when using a ferrite interposer, the same CPW shown in Fig. 3 is now simulated in the configuration shown in Fig. 4, where the bottom metal has been removed and an absorbing condition is applied. Note, that such a simulation topology is justified by the high losses introduced by the ferromagnetic interposer, which minimizes the coupling between the upper (CPW) and lower (wafer chuck) metals. Comparing the field intensity in Fig. 3 and Fig. 4 (plotted using the same intensity scale), a clear reduction of the transverse PPL mode can be seen.

B. CPW common mode

The CPW common mode occurs when an in-phase field across the transmission line gaps is present and can propagate, effectively creating a *leaky-wave* slot antenna [5]. The in-phase field arises from asymmetries in the structure geometry (i.e., manufacturing tolerances), imbalances in the stimuli (i.e., probe manufacturing tolerances and/or probe misplacements) or simply by a large physical separation of the two ground planes. Moreover, the CPW common mode can propagate due to the absence of direct (electrically short) contacts between the two ground stripes.

The effect of this mode on the wanted CPW differential mode can be represented as energy loss due to radiation. The amount of energy radiated is proportional to the electrical distance between the two CPW grounds and the gap width (i.e., related to $2 \cdot W_{Gap}+W_S$, the operating frequency and the substrate dielectric constant). Reducing the gap width effectively results in lowering the radiated energy, as shown in Fig. 5, where the gap is varied from 30µm to 15µm, and the structure is fed by a waveguide port.

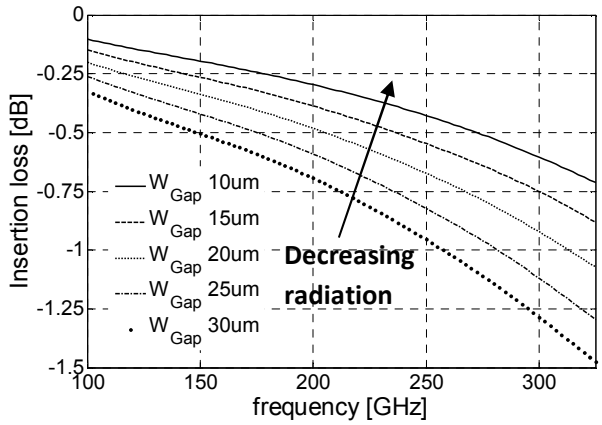

Fig. 5: Simulated insertion loss of CPW line described in Table I versus gap width, fixing the signal width to 47.5µm. The CPW line is excited by a waveguide port.

It is important to note that in a conventional CPW structure the characteristic impedance of the line (which is set close to 50 Ohm) is proportional to the ratio of $W_S/(W_S+2W_{Gap})$, thus when reducing the gap a given impedance can be achieved scaling the signal width. Nevertheless, when considering calibration structures, the need to preserve an homogenous CPW (i.e., no step in signal width), and the requirements on the minimum width of the signal line, capable to accommodate the probe tip dimension (i.e., ~20µm for classical probes), sets a limit to the minimum gap achievable on a given substrate. For this reason to minimize the gap, substrates with low ε_r should be chosen. This reduces the line capacitance per unit length allowing to achieve a smaller gap even when signal width and characteristic impedance are fixed.

C. Surface wave modes: TM_0 and TE_1

The surface waves modes propagate along the grounded dielectric slab, and have cut-off frequencies expressed by eq. 1. Their detailed analysis is beyond the scope of this paper, which focuses on showing the increased losses due to these higher order modes and their interference with the wanted CPW mode.

To study the overall loss behavior of the CPW structure when fed by a wafer probe, the 3D simulation environment shown in Fig. 6 is considered. A point voltage source with a source impedance of 50 Ohm is applied to the bridge to provide a transition similar to a wafer probe.

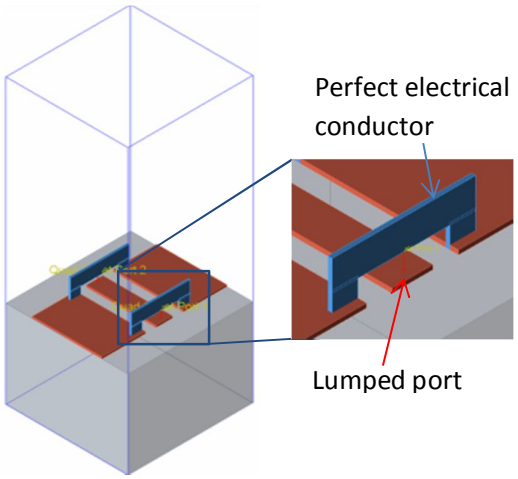

Fig. 6: 3D EM model of CPW and zoom-in of the lumped port used as stimulus, with boundary radiation box (blue box) directly set at the substrate edge (edge absorbing).

The S21 transfer between the input and output lumped ports (designed to couple the wanted CPW mode) is shown in Fig. 7.

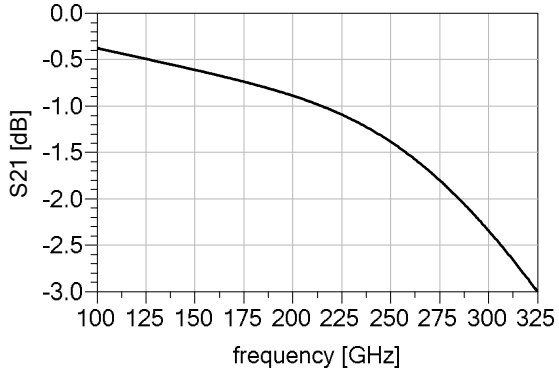

Fig. 7: Simulated S21 of CPW described in Table I when edge absorbing is considered (see Fig. 6).

Due to the absence of conductive and dielectric loss-mechanism in the structure, the drop in the S21 trace shown in Fig. 7 can only be attributed to energy dissipated in the other modes supported by the structure.

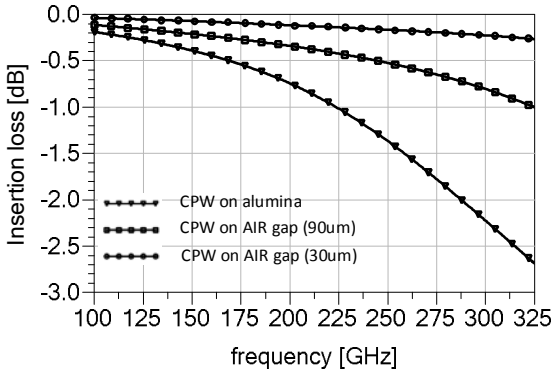

Fig. 8: Simulated insertion loss of the CPW structure described in Table I, compared to the air (ε_r=1) substrate case (CPW on AIR gap 30μm) and the case with air substrate and an increased gap to account for the guided wavelenght in the alumina (CPW on AIR gap 90μm).

Fig. 8 compares the insertion loss[1] of the CPW structure described in Table I with the same metal structure but over an air (i.e., ε_r=1) substrate. It can be seen by the figure that the loss mechanism for the CPW over air is fairly linear, since is dominated by the CPW common mode radiation (two gap sizes are shown). In the case of the CPW on alumina a change in the insertion loss slope around 175GHz can be noted. This is the frequency, see Fig. 2, where the CPW mode starts coupling with the TE_1 mode.

It is important to note that in the 3D simulation environment (Fig. 6), the boundary condition where set to absorbing, thus providing perfect match condition to all the unwanted modes within the structure.

[1] The insertion loss is used here to removes mismatch losses and provide a direct comparison accounting only for the radiation losses.

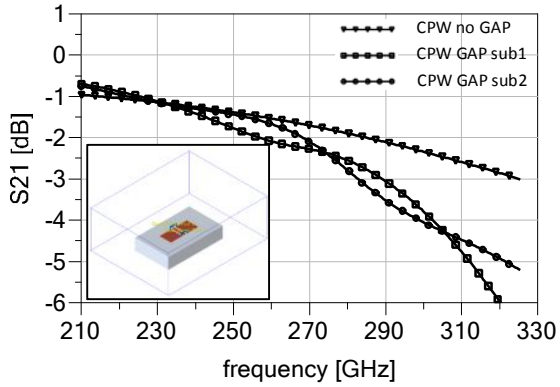

Fig. 9: Simulated S21 of CPW described in Table I for: case of structure shown in Fig. 6 (CPW no GAP), when the substrate island is enlarged of 320μm and a gap of 500μm is applied between the substarte and the absorbing box edge (CPW GAP sub1), and when substrate island is enlarged of 420μm and a gap of 500μm is applied between the substarte and the absorbing box edge (CPW GAP sub2).

A more realistic case can be obtained when the substrate is enlarged (i.e., 250μm after the CPW metal boundaries) and an air gap (500μm) between the substrate boundary and the radiation boundary of the box is applied, as show in the inset of Fig. 9. The finite dimension of the substrate will now present a dielectric constant discontinuity, thus providing an unmatched termination to the unwanted modes. This results in multiple reflections of the unwanted modes within the structure, generating an interference pattern (dependent on the distance to the discontinuity) along the trace, as can be seen in Fig. 9.

TABLE II: LINE AND SUBSTRATE PARAMETERS – FUSED SILICA -

Parameter	W_S	W_{Gap}	W_{GND}	d	ε_r
Value (in μm)	60	8	125	200	3.68
Metal: perfect electric conductor; *dielectric*: lossless fused silica					

IV. FUSED SILICA SUBSTRATE

The previous Sections described the energy loss/conversion from the primary intended mode (CPW even) to unwanted radiating modes in multimode transmission lines. The dependency of the radiating mode from the surroundings (e.g., dimension of the substrate, neighbor structures) makes the use of CPWs on electrically thick substrates (as the one considered in Table I) not accurate for calibration purposes.

Employing lower ε_r substrates shifts the occurrence of the TE_1, TM_1 modes to higher frequencies, and the amount of energy radiated by the CPW common mode can be reduced due to the smaller gap dimension for a given signal width. For these reasons fused silica [6], was considered as a good

candidate to integrate CPWs to perform TRL calibration in the (sub)mm-wave band (i.e., WR03).

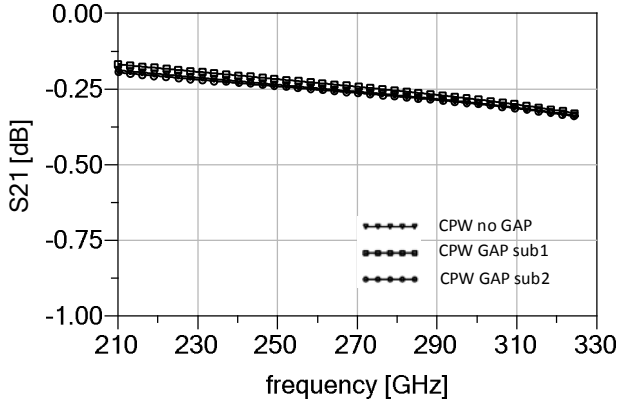

Fig. 10: Simulated S21 of CPW described in Table II for: case of structure shown in Fig. 6 (CPW no GAP), when substrate island is enlarged of 320 μm and a gap of 500μm is applied between the substarte and the absorbing box edge (CPW GAP sub1), and when substrate island is enlarged of 420 μm and a gap of 500μm is applied between the substarte and the absorbing box edge (CPW GAP sub2).

The same simulation analysis performed for the alumina case in Fig. 9 was carried out for the fused silica substrate, see Fig. 10. As can be seen by the plot a considerably lower amount of energy is transferred to other modes.

Moreover the lower dielectric constant of the substrate provides lower discontinuities when terminated with air, showing close to no-variation when an edge air model (see inset Fig. 9) is considered.

V. Experimental Results

A complete set of calibration structures were integrated on a 4 inch fused silica wafer [6] using the DIMES IC processing facilities, at the Delft University of Technology. The single mask process allowed a 2μm aluminum layer ,etched with photolithographic techniques providing a 0.5μm resolution.

The realized thru for the TRL calibration structures is shown in Fig. 11.

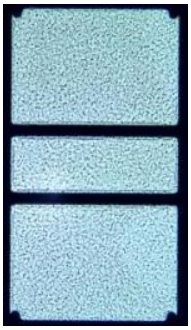

Fig. 11: Transmission line, as defined on Table II, integrated on the fused silica process.

The implemented structures were used to perform a full TRL calibration in the WR03 band (i.e., 220-325GHz) using an Agilent N5242A PNA-X network analyzer with OML Inc. frequency extender modules. The on-wafer structures were contacted using 100μm GSG GGB probes.

The VNA was calibrated using only the fused silica TRL structures and then employed to measure the lines of Table I and Table II. The measured data are then compared with the 3D EM simulation in Fig. 12 a and b for the fused silica and the alumina case, respectively. The plots show a good agreement between the simulation and the measured data, the small offset between the curves arises from the parasitcs (L and C) introduced by the bridge used in the simulation, which is removed from the measurements being a part of the calibration but is not removed from the simulated data. Note that the simulation for the fused silica now accounts for the losses in the metal and in the substrate.

When considering the real structures on alumina substrate (i.e., exhibiting also dielectric losses), it is expected that the lines closer to the edge of the substrate will exhibit a stronger ripple caused by interference with the surface wave mode. For this reason different structures where measured on different locations (i.e., center and edge) of the alumina substrate, and the results are reported in Fig. 13. As can be clearly seen by the figure, the structures at the edge of the substrate exhibit a clear interference pattern, as was also indicated by the simulation analysis of Section III, see Fig. 9.

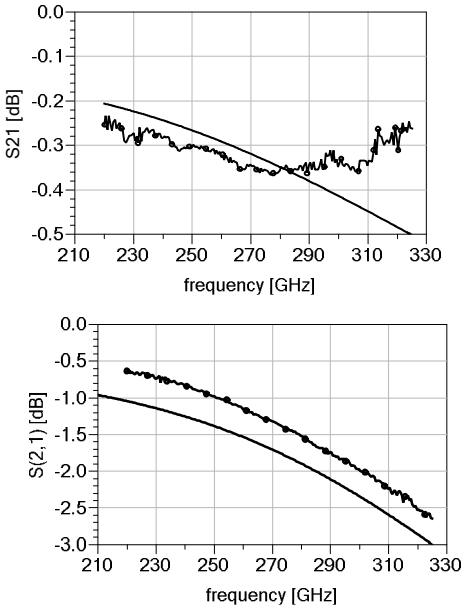

Fig. 12: Measured (line and symbols) and simulated data (solid line), after fused silica TRL calibration is performed. Measurement of structure from Table II, including metal and substrate loss (a), measurement of structure from Table I (b).

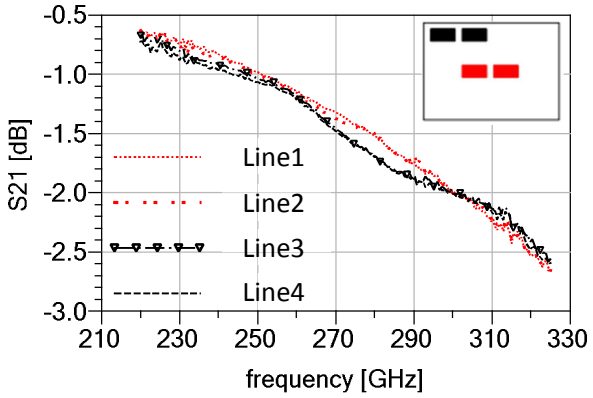

Fig. 13: Measurement of different (four) thru lines on alumina substrate in different location of the calibration substrate. Locations (i.e., two middle and two center) identified in the inset on top right.

In Fig. 14 the measured results of long lines implemented on alumina (1.8mm) and fused silica (1.68mm) are reported. The figure shows the lower amount of energy transferred to unwanted modes for the fused silica structure when compared to the alumina case, i.e., ~-1.1dB versus -10dB at 310GHz.

VI. Conclusion

In this paper an extensive analysis, based on 3D EM simulations, of the effect of multimode propagation occurring on CPW structures used for on-wafer calibration was given. The classical techniques to minimize the impact of some of the unwanted modes, occurring in the (sub)mm-wave range were described by means of numerical simulations and validated by experimental measurements.

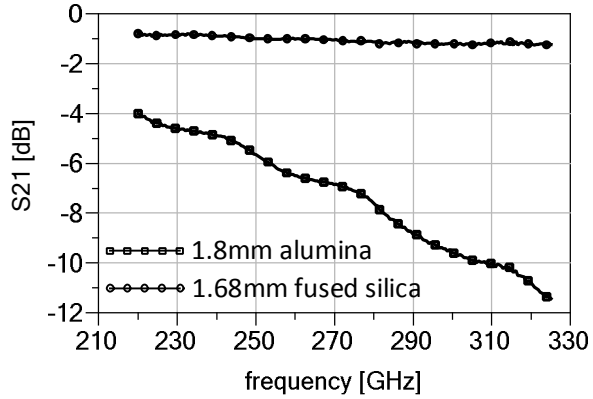

Fig. 14: Calibrated measured results of 1.8mm line on alumina and 1.68mm line on fused silica.

The limitations on the predictions of the electrical behavior of CPWs integrated on electrically thick substrates were discussed. A fused silica substrates was proposed and fabricated to perform accurate (sub)mm-wave calibration. Experimental data of CPW lines on both fused silica as well as alumina, acquired after a TRL calibration employing fused silica structures, demonstrate high correlation with their simulated data (i.e., 3D EM simulation). These results validate the accuracy of the performed calibration and the choice of fused silica as a substrate for (sub)mm-wave calibration.

Acknowledgement

The authors would like to thank Giuseppe Fiorentino from the DIMES research institute at the Delft University of Technology for the fabrication of the fused silica structures. This research work is supported by the CATRENE – CT209 – RF2THZ SiSOC project.

References

[1] F.J. Schmückle, R. Doerner, G.N. Phung, W. Heinrich, D. Williams, U. Arz, "Radiation, Multimode Propagation, and Substrate Modes in W-Band CPW Calibration", Proc. 41th European Microwave Conf., 2011, pp. 297-300.

[2] D. M. Pozar, Microwave Engineering 4th edition. John Wiley and Sons, 2012.

[3] H. Shigesawa, M. Tsuji, and A. A. Oliner, "A new mode-coupling effect on coplanar waveguides of finite width," IEEE MTT-S International Microwave Symposium Digest, vol. 3, pp. 1063–1066, 1990.

[4] R.W. Jackson, "Mode conversion at discontinuities in finite-width conductor-backed coplanar waveguide," Microwave Theory and Techniques, IEEE Transactions on , vol.37, no.10, pp.1582,1589, Oct 1989.

[5] J. L. Volakis, Antenna Engineering Book, 4th edition, McGraw-Hill, 2007, ch. 11.

[6] Nikon Corporation, Synthetic Silica Glass (Online). Available: http://www.nikon.com/products/glass/index.htm.